The electron-density distribution and chemical bonding of A15-type Cr obtained by the maximum-entropy method

1994 J. Phys.: Condens. Matter 6 8681

(http://iopscience.iop.org/0953-8984/6/42/001)

J. Phys.: Condens. Matter 6 (1994) 8681–8690. Printed in the UK

The electron-density distribution and chemical bonding of A15-type Cr obtained by the maximum-entropy method

H Ishibashi†, M Arita‡, I Nishida§, A Yanase† and K Nakahigashi†

† College of Integrated Arts and Sciences, University of Osaka Prefecture Sakai, Osaka 593, Japan

‡ Faculty of Technology, Nagoya University, Furo-cho, Chikusa-ku, Nagoya 464-01, Japan

§ Faculty of Science, Nagoya University, Furo-cho, Chikusa-ku, Nagoya 464-01, Japan

Received 13 June 1994

Abstract. The electron-density distribution of A15-type Cr was obtained by a combination of powder-x-ray-diffraction data and the maximum-entropy method (MEM). Fine powder, in which about 13 vol% BCC Cr was contained, prepared by evaporation of Cr in a low-pressure atmosphere of Ar, was used. Though the powder is composed of the two phases, the final R and R_W factors were 0.21% and 0.29%, respectively, and therefore excellent MEM maps were obtained. The MEM maps indicate that the main interaction is a strong covalent bond between adjacent 6c-site Cr atoms within the infinite linear chains. The MEM maps are compared with the valence-electron-density maps of superconducting V_3Si and non-superconducting Cr_3Si having an A15-type structure.

The structure factors for some forbidden reflections, which originate from asymmetric bonding-charge distribution, were also calculated from the MEM densities.

1. Introduction

A new modification of Cr was discovered for the first time by Kimoto and Nishida [1] in the fine particles prepared by evaporation in argon at low pressures. On the other hand, Forssell and Persson [2, 3] found this as a growth phase in the very thin films condensed on ultrahigh-vacuum-cleaved NaCl and KCl crystals and investigated the crystal structure based on the electron-diffraction data. They reported that the crystal structure of this new modification of Cr was a genuine A15 type with the space group $Pm\bar{3}n$. Thus the A15-type Cr exists only in fine particles or thin films together with BCC Cr and further this structure easily translates to BCC above 450 °C. Therefore almost all investigations of A15-type Cr hitherto reported were done by means of electron microscopy and electron diffraction except for the measurement of magnetic properties by Matsuo *et al* [4]. For example, the crystal habits of the A15-type Cr were examined by Nishida and Kimoto [5] and correspond to the icositetrahedron bounded by 24 {211} planes or the rhombic dodecahedron bounded by 12 {110} planes. However the other physical properties are unknown, therefore further studies of A15-type Cr, for example, the electron-density distribution in the crystal, are worth making.

On the other hand, the macroscopic and microscopic physical properties of the compounds for a formula A_3B with the A15-type structure have been investigated. Testardi [6] has reviewed the extensive literature on the experimental and theoretical studies of the physical properties, such as structural instability and high superconducting temperature, in binary and pseudobinary compounds exhibiting the A15-type structure. Staudenmann *et al*

0953-8984/94/428681+10$19.50

[7] and Staudenmann [8] examined the deformation and valence-electron-density distribution in the superconducting V_3Si and non-superconducting Cr_3Si with A15-type structure based on the single-crystal x-ray-diffraction data at room temperature. They reported that the strong covalent bond between adjacent V atoms in the former compound within the infinite linear chains was found as the main interaction. On the other hand, the Cr–Cr chain in the latter compound appears as a pile-up of charged atoms without bonding.

Recently, the maximum-entropy method (MEM) has been widely applied to draw the electron- and nucleus-density-distribution map for known structures from powder x-ray- or neutron-diffraction data. For example, Sakata's group examined this vigorously basing their analysis on both x-ray- and neutron-diffraction data [9–12]. Our group also reported previously the maps of AlN [13], Ge [14] and Ln_2O_3 (Ln = Y, Tm, Yb) [15]. In particular, in the case of AlN, two kinds of AlN powder, namely pure AlN powder and AlN powder in which 69 vol% Al was contained, were used. Nevertheless, the electron-density-distribution maps for the two kinds of powder agreed well.

The present paper gives the results of the study of the electron-density map and the bonding character of the A15-type Cr.

2. Experimental details

The details of the sample preparation of Cr fine particles are given in [1]. The Cr fine powder was prepared by evaporation of bulk Cr with purity 99.995% in an Ar atmosphere at about 1.3 kPa pressure. According to a preliminary work on x-ray diffraction, the powder thus prepared was composed of A15-type and BCC Cr. Powder-diffraction-intensity data were collected at room temperature with a tube voltage of 50 kV and a tube current of 240 mA by a Rigaku RINT 1500-type x-ray diffractometer equipped with a curved pyrolytic-graphite diffracted-beam monochromator. The x-ray measurement was carried out by step scanning with a sampling interval of 0.02° in 2θ and an accumulation time of 50 s for every step. The scan range in 2θ was $35° \leqslant 2\theta \leqslant 145°$ for Cu Kα radiation. By these experimental conditions, 13 and 6 Bragg reflections, respectively, for A15-type and BCC Cr were observed. The average particle size of the A15-type Cr was determined as about 700 Å from the dependence of the full width at half maximum (FWHM) on the value of the scattering vector for each Bragg reflection by the Scherrer equation. This seems to be suitable to obtain accurate intensity data free from the extinction effect.

3. The determination of integrated intensity

In order to determine the accurate integrated intensities of respective reflections from the powder-x-ray-diffraction-intensity data, a whole-powder-pattern fitting was carried out without using any structural model with the computer program WPPF by Toraya [16]. Since the peak asymmetry and different decay rates of the low- and high-angle sides of the peak can be modelled explicitly, a split Pearson VII function was adopted as a profile function in this program. In this procedure, the integrated intensities of respective reflections and the unit-cell parameters were refined. Figure 1 shows the powder pattern observed (top) at room temperature and the one calculated (bottom) by the pattern fitting, together with differences between the observed and calculated intensities. The notations $\delta(hkl)$ and $\alpha(hkl)$ in the figure indicate the reflections hkl of A15-type Cr and BCC Cr, respectively. The final R and R_W factors were 1.8% and 2.8%, respectively, and the refined unit-cell parameter of the

A15-type Cr was 4.600 89(3) Å. The twelve independent and one combined (432 and 520 reflections) integrated intensities thus determined are listed in the second column of table 1 together with their estimated standard deviations in parentheses. The volume fraction of A15-type Cr in the powder used was estimated by the same method as described previously [13, 17] using the integrated intensities of A15-type Cr and BCC Cr, the linear absorption coefficient and the unit-cell volume. The volume fraction of A15-type Cr thus determined was about 87%. Though we used the fine powder composed of the two phases, the observed integrated intensities shown in table 1 seem very precise and reliable. This is due to the non-existence of severely overlapping peaks.

Table 1. The observed integrated intensities I_{obs}, the observed structure factors F_{obs} and G_{obs} and the calculated structure factors F_{calc} from the MEM map.

hkl	I_{obs}	F_{obs}	F_{calc}	
200	1336(2)	70.46(19)	70.34	
210	3698(4)	−66.50(17)	−66.16	
211	2733(3)	63.49(16)	63.29	
222	254(1)	−49.76(16)	−49.77	
320	662(2)	48.34(14)	48.54	
321	1169(2)	47.07(13)	47.33	
400	462(1)	88.38(26)	88.43	
420	340(1)	39.81(12)	39.82	
421	642(2)	−38.72(11)	−38.75	
332	314(1)	38.11(12)	38.04	
521	734(2)	33.43(10)	33.40	
440	899(3)	65.32(20)	65.25	
432	1009(2)	$G_{obs} = 33.53(9)$	33.10	$G_{calc} = 33.51$
520			34.32	

4. The crystal structure refinement and deduction of structure factors

In the next step, the scale factor has to be determined in order to convert the integrated intensities into the structure factors on an absolute scale. This process was accomplished by an ordinary least-squares analysis using, for example, the computer program POWLS [18]. In the first stage of the least-squares refinement, the effects on the anharmonic thermal vibration and the preferred orientation were considered. However, their effects slightly changed the value of the scale factor within its estimated standard deviation; therefore, they were neglected in the present calculation. This negligibly small preferred-orientation effect is consistent with the crystal habit observed by electron microscopy [4], namely the shape of the A15-type Cr is neither needle like nor plate like; rather it is nearly sphere like.

The crystal structure of the A15-type Cr hitherto reported was determined by electron diffraction and/or the Debye pattern of x-ray diffraction [1, 3]. We refined, for the first time, the crystal structure of the A15-type Cr. The eight Cr atoms are contained in a unit cell of A15-type structure and placed at special positions as follows:

Cr(1) 2a site 000, $\frac{1}{2}\frac{1}{2}\frac{1}{2}$

Cr(2) 6c site $\frac{1}{4}0\frac{1}{2}$, $\frac{1}{2}\frac{1}{4}0$, $0\frac{1}{2}\frac{1}{4}$

$\frac{3}{4}0\frac{1}{2}$, $\frac{1}{2}\frac{3}{4}0$, $0\frac{1}{2}\frac{3}{4}$.

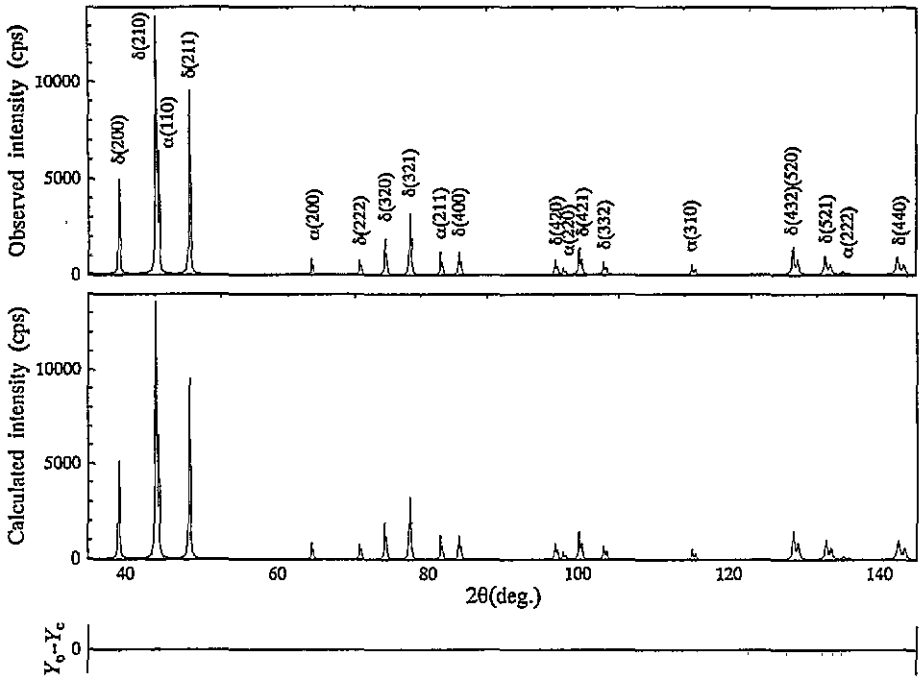

Figure 1. The observed (top) and calculated (bottom) intensities of the Cr fine powder. The differences between the two intensities are plotted at the bottom. The notations $\delta(hkl)$ and $\alpha(hkl)$ indicate the hkl reflections of A15-type Cr and BCC Cr, respectively.

Consequently, the parameters that have to be refined in this analysis are the scale factor and the isotropic temperature factors at each position. The results of the least-squares analysis are tabulated in table 2 together with the R and R_W factors. We note here that no other structure models gave a smaller R factor than the A15-type structure.

Table 2. A summary of the results of the least-squares refinement by POWLS.

Number of data used in POWLS analysis	13
Independent reflections	12
Combined reflections	1
Isotropic temperature factor of Cr at 2a site (Å^2)	0.12(3)
Isotropic temperature factor of Cr at 6c site (Å^2)	0.18(2)
Scale factor	0.576(3)
R factor	0.0051
Weighted R factor	0.0092

The observed independent structure factors $F_{obs}(k)$ are straightforwardly calculated from the observed integrated intensities by using the scale factor. The overlapped reflection of 432 and 520, however, was treated as the combined structure factor $G_{obs}(j)$, which was obtained by taking a square root of the observed integrated intensity after the ordinary corrections and scaling. The phases of the structure factors have no ambiguities because of an inversion symmetry. The structure factors thus determined include the effect on the anomalous dispersion. Therefore, the effect was eliminated from the structure factors by

using the values of anomalous-dispersion-correction terms given in [19]. The results for the structure factors $F_{obs}(k)$ and $G_{obs}(j)$ are also tabulated in the third column of table 1 together with their estimated standard deviations $\sigma(k)$ and $\sigma(j)$.

5. The MEM analysis and the MEM map of A15-type Cr

The procedure of the MEM calculation is the same as in previous reports [9–15]; therefore, we only briefly explain here the MEM analysis using x-ray-powder data. The constraint C is defined as

$$C = \frac{1}{N_1 + N_2}\left[\sum_{k}^{N_1} \frac{|F_{calc}(k) - F_{obs}(k)|^2}{\sigma^2(k)} + \sum_{j}^{N_2} \frac{|G_{calc}(j) - G_{obs}(j)|^2}{\sigma^2(j)}\right] \quad (1)$$

where N_1 and N_2 are the numbers of observed independent structure factors and combined ones, respectively. Moreover, $F_{calc}(k)$ and $G_{calc}(j)$ are the calculated structure factors given as

$$F_{calc}(k) = V\sum_{r} \tau(r)\exp(-2\pi r \cdot k) \quad (2)$$

$$G_{calc}(j) = \left[\sum_{k} m(k)|F_{calc}(k)|^2 \Big/ \sum_{k} m(k)\right]^{1/2} \quad (3)$$

where V is the unit-cell volume, $\tau(r)$ is the prior electron density at a certain pixel located at r and $m(k)$ is the multiplicity of the structure factor $F(k)$. By solving the MEM equation, the electron density $\rho(r)$ can be written as

$$\rho(r) = \exp\left[\ln\tau(r) + \frac{\lambda F_0}{N_1 + N_2}\left\{\sum_{k} \frac{F_{calc}(k) - F_{obs}(k)}{\sigma^2(k)}\exp(2\pi i r \cdot k) + \sum_{j} \frac{G_{calc}(j) - G_{obs}(j)}{\sigma^2(j)G_{calc}(j)\sum_k m(k)} \sum_{k} m(k)F_{calc}(k)\exp(-2\pi i r \cdot k)\right\}\right] \quad (4)$$

where λ is the Lagrange undetermined multiplier and F_0 is the total number of electrons in a unit cell, namely 24×8 in the present case. Starting from uniform density, the electron densities $\rho(r)$ were iteratively calculated using (4) and the data set shown in table 1 until the condition $C \leqslant 1$ was satisfied. The number of pixels used in the calculation was $64 \times 64 \times 64$. The actual calculation, however, was done in the region of the minimum asymmetric unit, written as $0 \leqslant x \leqslant \frac{1}{2}$; $0 \leqslant y \leqslant \frac{1}{2}$; $0 \leqslant z \leqslant \frac{1}{4}$; $z \leqslant \min(x, \frac{1}{2} - x, y, \frac{1}{2} - y)$ [20]. This procedure reduced the number of pixels to 6017. The actual calculation of the MEM density was performed with the computer program MEED by Kumazawa *et al* [21].

The calculated structure factors $F_{calc}(k)$ from the final MEM density distribution are also tabulated in the last column of table 1. In the present calculation, the values of R and R_W factors attained at the final MEM map were 0.21% and 0.29%, respectively. The agreement of observed and calculated structure factors is very good, though we used the powder sample composed of two phases. The electron-density-distribution maps of the lower- and higher-density regions for the (001) plane are shown in figure 2(*a*) and (*b*), respectively, where the 2×2 unit cells are drawn in order to demonstrate the bonding character. As is clear

from figure 2(*a*), the electron-density distribution around 6c-site Cr atoms (Cr(2)) is quite different from that around 2a-site Cr atoms (Cr(1)). The tight covalent bonding between the adjacent Cr(2) atoms within the infinite linear chains is clearly found, and the peak height at the middle point between adjacent Cr(2) atoms is 0.9 e $Å^{-3}$. The electron densities observed around the points such as $0\frac{1}{2}0$ show a cross section of the linear chains along the z axis. Furthermore, the electron-density distribution about the Cr(2) atoms spreads in the direction perpendicular to the linear chains. On the other hand, the asphericity of the electron-density distribution around the Cr(1) atom is characterized by the spread towards the centre of the adjacent Cr(2) atoms. These facts may be an indication of the existence of a weak bond between the Cr(1) atom and the Cr(2)–Cr(2) bond. In contrast to the valence-electron distribution described above, the core-electron distribution is perfectly spherical as shown in figure 2(*b*). The peak height at the Cr(1) atoms is 349.1 e $Å^{-3}$, and at the Cr(2) atoms, the height is slightly smaller, i.e. 343.6 e $Å^{-3}$.

6. Discussion

Staudenmann [8] calculated, based on single-crystal x-ray diffraction data at room temperature, the deformation and valence-electron-density distribution of superconducting V_3Si and non-superconducting Cr_3Si compounds with A15-type structure. There are apparently three differences between them as follows [8]:

(i) the peak height (0.55 e $Å^{-3}$) of the electron density at the middle point between the two adjacent V atoms in V_3Si is about three times as large as that of Cr_3Si (0.17 e $Å^{-3}$);

(ii) V atoms in the infinite linear chains of V_3Si appear to be covalently bonded to one another, while Cr atoms in Cr_3Si appear as rows of charged atoms;

(iii) the valence-electron density of the Si atoms is deformed in the direction of the Cr atoms in Cr_3Si; it is directed towards the V–V bond in V_3Si.

As described in the previous section, a strong covalent bond between the adjacent Cr(2) atoms and a weak interaction between the Cr(1) and the Cr(2)–Cr(2) bond in the A15-type Cr are observed. Judging from only the electron-density distribution, therefore, V_3Si and A15-type Cr are quite alike. As is well known, V_3Si is a superconducting compound with $T_c = 17$ K. We also examined preliminarily a temperature dependence of the magnetic susceptibility of the present powder; however, no indications of a diamagnetic signal were observed down to 2 K. Staudenmann [22] studied the electron density distribution in a martensitically transformed single crystal of V_3Si and reported that the most significant difference between the electron-density maps at room temperature and below the superconducting transition temperature was the disappearance of the weak bond between the Si atom and the V–V bond on a chain at low temperature, so we are now planning to examine the electron-density maps of the A15-type Cr at low temperature. The peak height of the electron density at the middle point between the adjacent Cr(2) atoms was 0.9 e $Å^{-3}$. This value is about twice and three times as large as that of the V–V bond in V_3Si and the Ge–Ge bond in Ge [14], respectively. This stronger covalent bonding compared to the V–V bond in V_3Si, the Cr–Cr bond in Cr_3Si and the Ge–Ge bond in Ge may be considered to reflect their electric nature.

In order to examine the accuracy level of the MEM maps of A15-type Cr, the influence of the misestimation of the scale factor on the maps was investigated as reported previously [9]. In figure 3, the MEM map in a lower-density region than that shown in figure 2(*a*) is shown. We examined the MEM density-distribution maps by changing the scale factor within

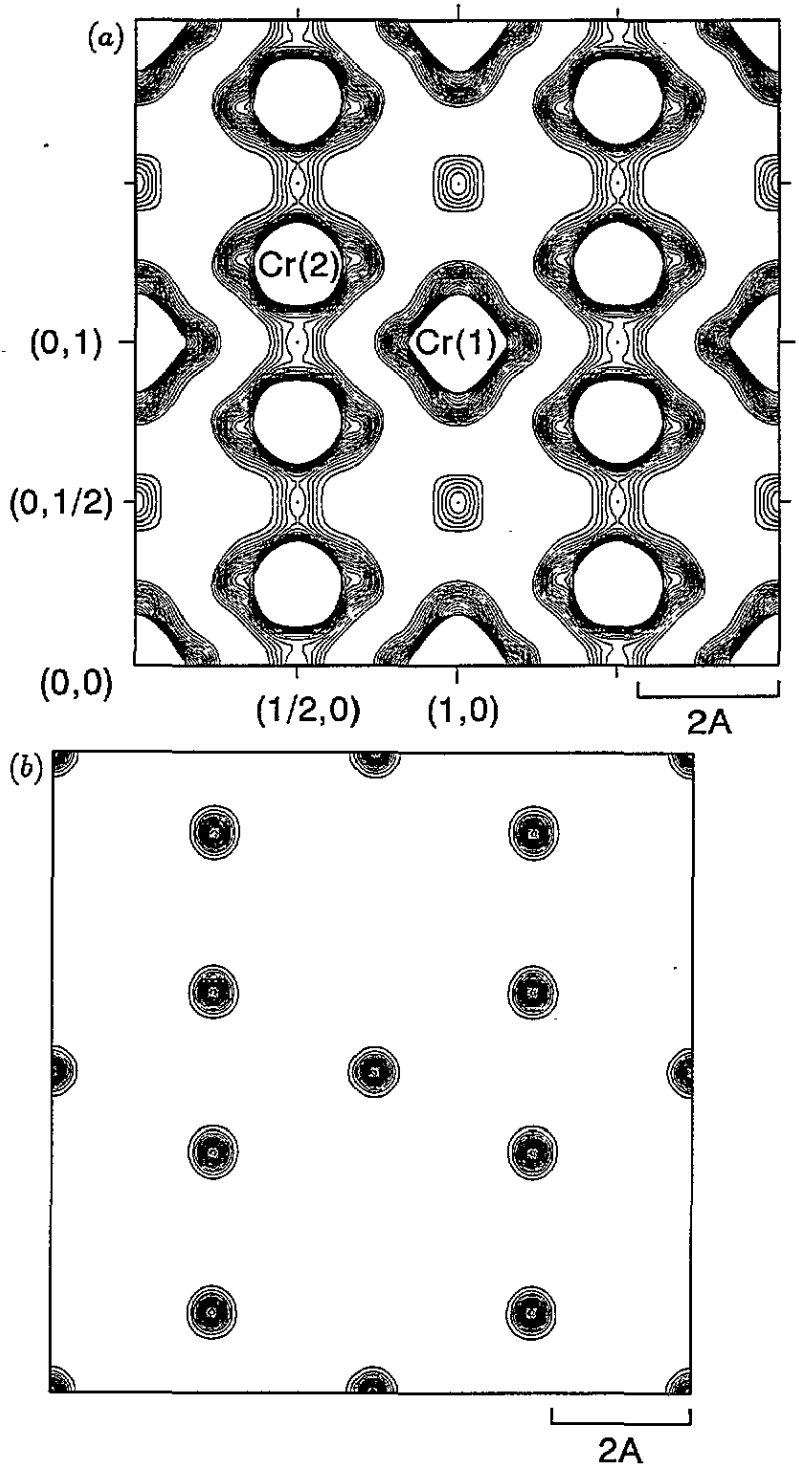

Figure 2. The MEM electron-density-distribution maps for the (001) plane of the A15-type Cr. (*a*) and (*b*) are the lower- and higher-density regions, respectively. The contour lines (e $Å^{-3}$) are drawn from 0.4 to 2.0 with 0.1 intervals in (*a*) and from 20.0 to 340.0 with 20.0 intervals in (*b*).

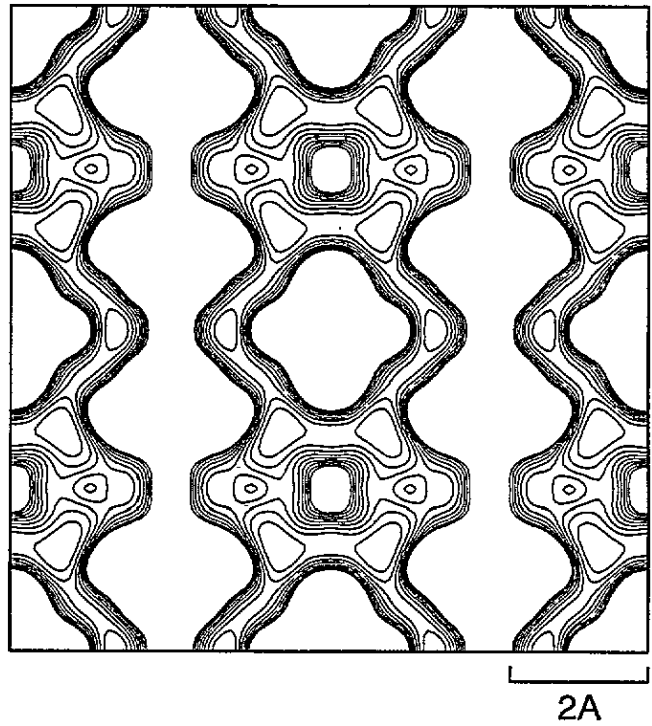

Figure 3. The MEM map of the (001) plane in a lower-density region than that shown in figure 2. The contour lines (e $Å^{-3}$) are drawn from 0.1 to 0.5 with 0.05 intervals.

$\pm 5\sigma$ where σ is the estimated standard deviation of the scale factor, though the scale factor was well refined in the least-squares refinement. Probably the values $\pm 5\sigma$ are the extreme cases of misestimation. The MEM maps of the same plane as shown in figure 3 for $+5\sigma$ and -5σ are shown in figure 4(*a*) and (*b*), respectively. No significant differences are seen except for the levels less than 0.3 e $Å^{-3}$. For the higher-density region, of course, the maps were in perfect agreement. Consequently, we are certain the MEM maps shown in figure 2 are very accurate. Some of the present authors calculated an energy band structure, Fermi surface and electron-density distribution of A15-type Cr using an FLAPW method and the results will be reported elsewhere. The calculated electron-density maps reproduced well, at least qualitatively, the MEM maps.

Table 3. The unmeasured structure factors calculated from the MEM map.

hkl	F_{calc}
110	0.51
220	0.49
310	0.28
410	−1.39
411	0.78
330	−0.47
422	−1.07
430	−0.50
510	0.01
431	0.75

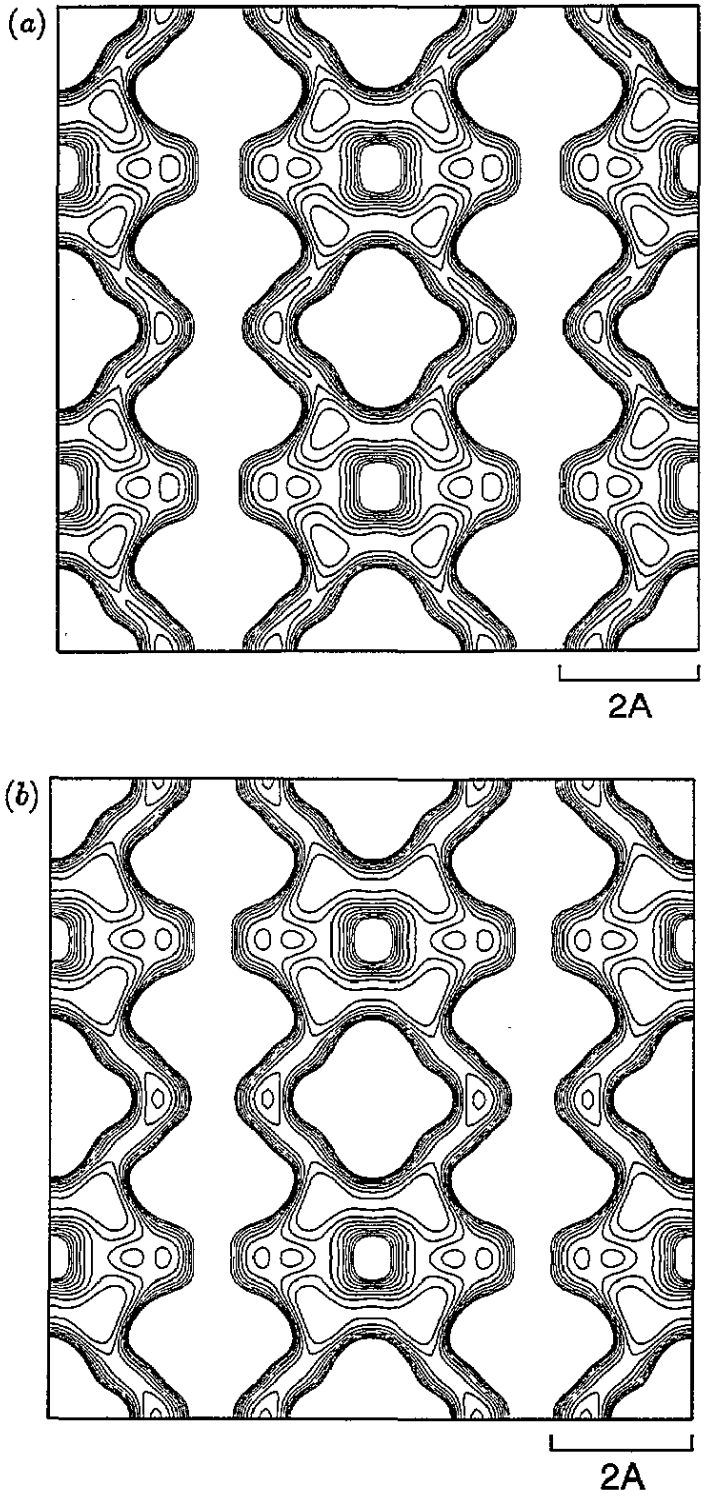

Figure 4. The MEM maps of the (001) plane calculated using the scale factor changed by (*a*) $+5\sigma$ and (*b*) -5σ. The contour lines are the same as in figure 3.

Borie [23] studied the structure factors of forbidden reflections of V_3Si using single-crystal x-ray-diffraction data. The values for 410 and 430 reflections were reported as 0.33 and 0.16, respectively. We can easily calculate the structure factors of the unmeasured reflections of the A15-type Cr from the MEM electron-density distribution. The calculation was done within the limiting sphere for Cu Kα radiation and the results, together with their signs, are tabulated in table 3. These reflections are not usually observed because of the extinction rules. The absolute values for 410 and 430 reflections of the A15-type Cr are about four and three times, respectively, as large as those of V_3Si. This fact predicts the differences between the A15-type Cr and V_3Si in anharmonic and anisotropic thermal vibrations together with their non-spherical electron-density distributions.

Acknowledgments

All the computations were carried out at the General Information Centre of the University of Osaka Prefecture. The authors thank Professor M Sataka of Nagoya University and Dr S Kumazawa of the Science University of Tokyo for allowing them to use the computer programs related to the MEM.

References

[1] Kimoto K and Nishida I 1967 *J. Phys. Soc. Japan* **22** 744–56
[2] Forssell J and Persson B 1969 *J. Phys. Soc. Japan* **27** 1368–9
[3] Forssel J and Persson B 1970 *J. Phys. Soc. Japan* **29** 1532–45
[4] Matsuo S, Nishida I, Kimoto K and Noguchi S 1978 *J. Phys. Soc. Japan* **44** 1387–8
[5] Nishida I and Kimoto K 1974 *Thin Solid Films* **23** 179–89
[6] Testardi L R 1975 *Rev. Mod. Phys.* **47** 637–48
[7] Staudenmann J L, Coppens P and Muller J 1976 *Solid State Commun.* **197** 629–33
[8] Staudenmann J L 1977 *Solid State Commun.* **23** 121–5
[9] Sakata M, Mori R, Kumazawa S, Takata M and Toraya H 1990 *J. Appl. Crystallogr.* **23** 526–34
[10] Sakata M, Uno T, Takata M and Mori R 1992 *Acta Crystallogr.* B **48** 591–8
[11] Sakata M, Uno T, Takata M and Howard C J 1993 *J. Appl. Crystallogr.* **26** 159–65
[12] Kubota Y, Takata M and Sakata M 1993 *J. Phys.: Condens. Matter* **5** 8245–58
[13] Nakahigashi K, Ishibashi H and Minamigawa S 1993 *J. Phys. Chem. Solids* **54** 445–52
[14] Nakahigashi K, Higashimine K, Ishibashi H and Minamigawa S 1993 *J. Phys. Chem. Solids* **54** 1543–8
[15] Ishibashi H, Shimomoto K and Nakahigashi K 1994 *J. Phys. Chem. Solids* at press
[16] Toraya H 1986 *J. Appl. Crystallogr.* **19** 440–7
[17] Nakahigashi K, Ishibashi H, Minamagawa S and Kogachi M 1992 *Japan. J. Appl. Phys.* **31** 2293–8
[18] Will G, Parrish W and Huang T C 1983 *J. Appl. Phys.* **16** 611–22
[19] 1993 *International Tables for Crystallography* vol C, ed A J C Wilson (Dordrecht: Kluwer) p 220
[20] 1993 *International Tables for Crystallography* vol A, ed T Mahn (Dordrecht: Kluwer) p 670
[21] Kumazawa S, Kubota Y, Takata M, Sakata M and Ishibashi Y 1993 *J. Appl. Crystallogr.* **26** 453–7
[22] Staudenmann J L 1978 *Solid State Commun.* **26** 461–8
[23] Borie B 1981 *Acta Crystallogr.* A **37** 238–41